Sensing and Bio-Sensing Research 2 (2014) 38–42

Contents lists available at ScienceDirect

Sensing and Bio-Sensing Research

journal homepage: www.elsevier.com/locate/sbsr

An in-line fiber-optic modal interferometer for simultaneous measurement of twist and ambient temperature

Yongqin Yu [a,b,*], Quandong Huang [c], Xuejin Li [a,b], Xue Chen [c], Chenlin Du [c]

[a] College of Physics Science and Technology, Shenzhen Key Laboratory of Sensor Technology, Shenzhen University, China
[b] ShenZhen Engineering Laboratory for Optical Fiber Sensors and Networks, China
[c] College of Electronic Science and Technology, Shenzhen University, China

ARTICLE INFO

Keywords:
Photonic crystal fibers
Fiber optics sensors
Twist sensor
Temperature sensor

ABSTRACT

A novel and simple sensor based on fiber-optic modal interferometer fabricated by a segment of low elliptical hollow-core photonic bandgap fiber for simultaneous temperature and twist measurements is demonstrated. Meanwhile the sensor can also measure the twist angle and determine the twist direction simultaneously. The mode distribution of EHC-PBGF is demonstrated both in theory and experiments. There is an obvious difference of two transmission dips on the temperature and twist. The twist sensitivities of Dip 1 and Dip 2 are obtained to be −31.95 and −585.8 pm/(rad/m), respectively. The temperature sensitivities are 12.99 pm/°C for Dip 1 and 5.09 pm/°C for Dip 2, respectively. Two parameters of twist and temperature can be distinguished and measured simultaneously by using a sensing matrix. Meanwhile the structure is found to be weakly sensitive to the axial strain. It has the advantage of avoiding the crosstalk of strain in the applications.

1. Introduction

Twist is an important sensing physical parameter that needs to be monitored in multi-area applications, such as detecting the health condition of engineering structure and mechanical equipment. And optical fiber sensors have the advantages of possessing a small size, easy to embed into the structures and anti-electromagnetic interference, et al. [1]. So far, there have been many works to study fiber sensor characteristic of twist/torsion, for example, twist sensors by using the birefringence of photonic crystal fiber [2–4] and long period fiber gratings (LPFGs) [5–7]. In 2011, a fiber ring laser incorporating a pair of rotary long-period grating was used for torsion sensing with a torsion sensitivity of 0.084 nm/(rad/m) in the torsion range ±100 rad/m [8]. In the same year, Chen WG reported a highly sensitive torsion sensor based on Sagnac interferometer using side-leakage photonic crystal fiber [9]. The achieved maximum torsion sensitivity is about 0.9354 nm/degree. Twist sensors, such as special fibers composed by carbon nanotube [10], fiber-optic polarimetric twist sensor [4], or special fluid filled in photonic crystal fiber [11], have been evolving to diversified applications. To our best acknowledge, twist fiber sensors with a low temperature cross-sensitivity have been reported above, while simultaneous sensing of twist and temperature based on fiber has not been reported, which may be have a potential twist applications for the real-time monitoring of the components working in harsh and complex conditions.

Since hollow core photonic bandgap fiber (HC-PBGF) was proved of light guiding in low index air core in 1999 [12], its unique merits [13–15] have been attracting scholars' attention to investigate for sensor applications, such as the employ of original hollow-core trait structure as Fabry-Pérot-type strain sensor [16–18], fabricating LPFG sensor by collapsing part of surrounding air-core [19], in-fiber polarimeters and Sagnac interferometer are reported [20,21], offset-splicing a single-mode fiber (SMF) with HC-PBGF as a inclinometer for detecting direction was also reported as a novel application [22].

In this paper, an in-line fiber-optic modal interferometer based on low elliptical hollow-core photonic bandgap fiber (EHC-PBGF) has been studied for simultaneous measurement of twist and temperature. This in-line fiber-optic modal interferometer is simply composed by directly splicing a section of EHC-PBGF with single-mode fibers (SMFs). The mode distribution of EHC-PBGF is demonstrated both in theory and experiments. The sensitivities of temperature and twist are investigated. Utilizing the obvious difference of two transmission dips on temperature and twist, two parameters can be simultaneously distinguished and

* Corresponding author at: College of Physics Science and Technology, Shenzhen Key Laboratory of Sensor Technology, Shenzhen University, China.
E-mail address: yuyq@szu.edu.cn (Y. Yu).

http://dx.doi.org/10.1016/j.sbsr.2014.10.013
2214-1804/

measured by using one single modal interferometer. Meanwhile the twist direction can also be distinguished. Moreover, we find that the structure is weakly sensitive to the axial strain. It has the advantage of avoiding the crosstalk of strain and this structure is simple and easy to be fabricated as well.

2. Experimental setup

Scheme of experimental setup for simultaneous measurement of twist and temperature is shown in Fig. 1(a). A broadband light source, generated by a superluminescent light-emitting diode (SLED) (LIGHT COMM Inc. China) and an optical spectrum analyzer (OSA, YOKOGAWA AQ6370B) are connected to the sensing component to monitor the transmission spectra as applied physics parameters vary. The sensing component is composed of a section of EHC-PBGF spliced with SMFs. EHC-PBGF is fabricated and supported by Yangtze Optical Fiber and Cable Corporation in China. Scanning electron micrograph (SEM) image of its cross section is shown in Fig. 1(b) and its local enlarged image is shown in Fig. 1(c). The dark areas are the air holes and the bright areas are solid silica. The maximum dark area in the center is air core which is a low elliptical geometry with a long axis of 7.5 μm and a short axis of 6.9 μm, which indicates that it is a low-birefringence fiber, while six solid silica rods distributing around the air core are high birefringence due to their asymmetric structures, as shown in Fig. 1(c) by six red circle lines. The cladding is with a diameter of 125 μm. And the pitch of air holes surrounding the air core is about 4 μm. Fig. 1(d) shows the photograph of the segment of EHC-PBGF with a length of 651.8 μm that captured by optical microscope (Olympus BX51, Olympus Inc.). It can be seen that there is no obvious collapse in the air holes. Both ends of EHC-PBGF were spliced with SMFs by using a FETEL S178A fusion splicer; and all the splicing process was done manually by controlling the appropriate arc intensity and arc duration to protect collapse of air-core and realize a high splicing strength. We firstly spliced one end of EHC-PBGF with a SMF and cut off the other end under the optical microscope by remaining a needed length and then spliced the remaining EHC-PBGF with a SMF.

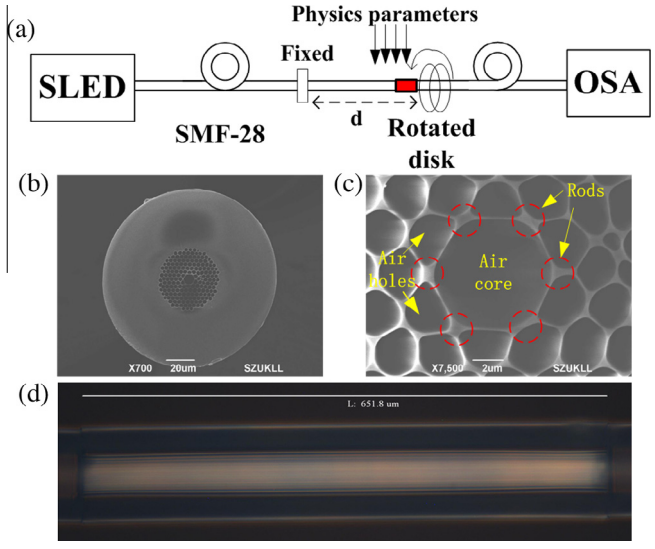

Fig. 1. (a) Scheme of experimental setup. SLED: superluminescent light-emitting diode, OSA: an optical spectrum analyzer; (b) Cross section SEM image of EHC-PBGF. (c) Local enlarged SEM image of the core region. Six solid silica rods distributing around the air core labeled in red dotted circle lines. (d) Photograph of EHC-PBGF with a length of 651.8 μm spliced with SMFs. (For interpretation of the references to colour in this figure legend, the reader is referred to the web version of this article.)

The propagation loss of EHC-PBGF is measured by the cutback method. The transmission spectra of EHC-PBGF with lengths of 0.6 and 1.2 m are obtained firstly using the same splicing conditions, as shown in Fig. 2. Then the propagation loss versus wavelength is obtained by subtraction and normalization as shown in Fig. 2 in blue color. There is a cut-off region of photonic bandgap located from 1360 to 1416 nm. The propagation loss at 1550 nm is obtained to be about 4.3 dB/m and the splicing loss between EHC-PBGF and SMF-28 is about 7.0 dB at 1550 nm. The high average insert loss we considered results by two reasons. Firstly, the homogeneous distribution of air holes in the cladding is not good, which leads to the weak photonic bandgap effect of EHC-PBGF and secondly the core is mismatched between EHC-PBGF and SMFs. The insertion loss is much higher in the short wavelength region because of the poorer bandgap effect. So in the sensing experiments, we only record the transmission spectra of EHC-PBGF in the long wavelength region.

The photographs in Fig. 3(a) and (b) show near field mode distribution of EHC-PBGF at 1550 nm captured by infrared microscope (Leica DM6000M, Leica Inc.) with a tunable laser. It indicates the existing LP_{01} and LP_{11} in the air core and cladding supermode in the solid silica rods. A full-vector finite element method with the commercial software COMSOL Multiphysics was applied to simulate the modal characteristic of EHC-PBGF. The photographs shown in Fig. 4(a) and (b) show the two core modes of LP_{01} and LP_{11} at the wavelength of 1550 nm and the supermodes distributed in the solid silica rods are clearly co-existing. Comparing Figs. 3 and 4, we can see the experimental results and simulated results are well consistent.

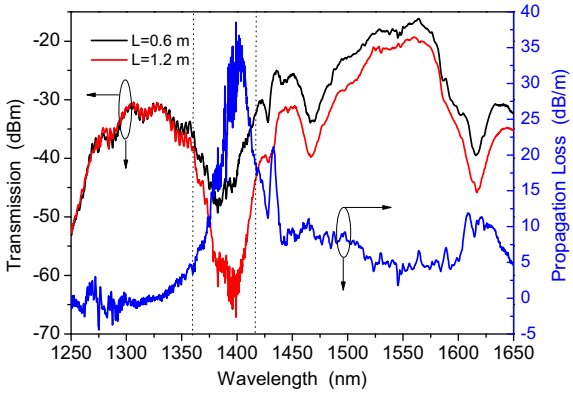

Fig. 2. Transmission spectra of EC-PBGF with lengths of 0.6 m (black line) and 1.2 m (red line), respectively. The propagation loss versus wavelength (blue line). A cut-off region lies between two dash lines. (For interpretation of the references to colour in this figure legend, the reader is referred to the web version of this article.)

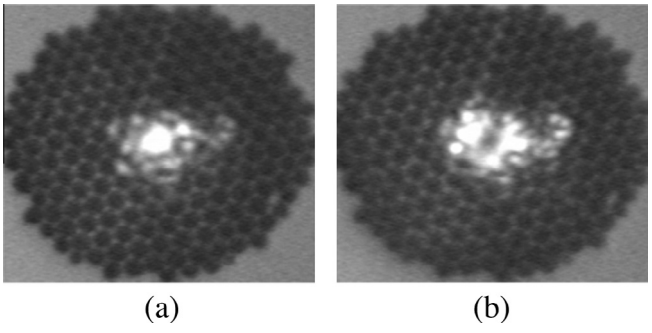

Fig. 3. The near field mode distribution captured by infrared microscope at the wavelength of 1550 nm. (a) LP_{01}, (b) LP_{11}; some supermodes in six bar-type silica rods of the cladding are also observed.

For a modal interference, the accumulated phase difference of different modes with the propagational length of L can be expressed as $\varphi = 2\pi\Delta n_{eff}L/\lambda$, here λ is the operating wavelength, Δn_{eff} is the effective refractive index difference of the two modes that propagated in the core or cladding. When the phase difference satisfies the condition $\varphi = (2m+1)\pi$, a resonant dip appears at:

$$\lambda_m = 2\Delta n_{eff}L/(2m+1) \quad (1)$$

where m is an integer. When the surrounding physical parameters are applied on the modal interference, the phase difference between the two modes will be changed, which indicates the wavelength shift of the interference dip.

3. Results and discussion

The transmission spectrum of the modal interferometer with a length of 651.8 μm and without twist at room temperature is shown in Fig. 5. The maximum fringe visibility of the interference resonance dips is 19.1 dB. Moreover, some minor dips can also be observed, which indicates that multiple modes contribute to the interference [17] and it is an interference superposition of some modes. In Fig. 5, there are two dips marked by Dip 1 at wavelength of 1446 nm and Dip 2 at wavelength of 1545 nm, respectively, which are recorded in the sensing experiments rather than other dips due to these two dips are cleanly and easily distinguished with high contrast and not overlapped by other dips.

The response of the modal interferometer with a length of 651.8 μm to twist was investigated experimentally. The EHC-PBGF under test is positioned at the middle of a section of fiber, and then

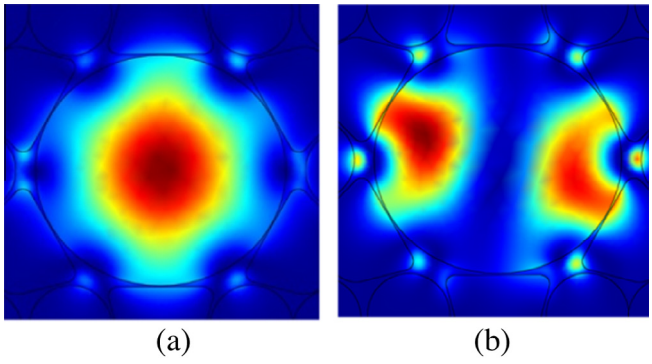

Fig. 4. The mode field distribution simulated by using COMSOL at the wavelength of 1550 nm. (a) LP_{01} and (b) LP_{11}.

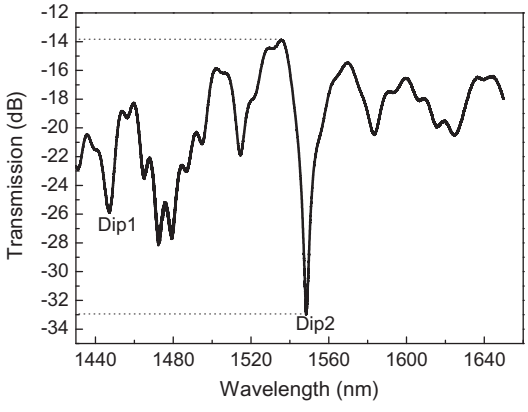

Fig. 5. The transmission spectrum of EHC-PBGF with a length of 651.8 μm.

one end of the fiber is fixed on a fiber holder, the other end is stuck in a rotated disk and the total twist length d is set to10 cm, as shown in Fig. 1(a). Fig. 6(a) shows the transmission spectra of the modal interferometer at two anti-clockwise twist rates of 0 and 2.618 rad/m. Two resonance dips marked by Dip 1 and Dip 2 are clear. It can be seen that the center wavelength of Dip 1 remains almost still, while the resonant wavelength of Dip 2 is red-shift when the twist rate applies from 0 to 2.618 rad/m. Fig. 6(b) shows the dependence of wavelength shift upon the twist rate. Firstly, the fiber is twisted in anti-clockwise in a total angle of 25 degree by step of 5 degree and then turned back to the original point for clockwise twist experiment. As shown in Fig. 6(b), when the fiber is twisted anti-clockwise, wavelengths of resonance Dip 1 and Dip 2 are both redshift, and while twisted clockwise, the wavelengths are both blueshift, and it is completely reversible and repeatable in our experiments. Obviously, the wavelength shift of Dip 1 at 1446 nm is dependent weakly on the twist; on the other hand, Dip 2 at 1545 nm is stronger dependent on the twist. By using linear fit, the twist sensitivities of Dip 1 and Dip 2 are obtained to be −31.95 and −585.8 pm/(rad/m), respectively. It indicates the sensitivity of Dip 2 is much higher than that of Dip 1. We consider that Dip 1 is resulted from an interference of some supermodes in bar-type silica rods of the cladding. The high birefringence of the supermodes leads to the polarization maintaining of guided light. So the wavelength shift of Dip 1 is dependent weakly on the twist. While Dip 2 is resulted from the resonant interference of two guided air core modes with a low birefringence, which leads to that the wavelength shift is strongly dependent on the twist. In many papers published before, various high-birefringence fibers (HBFs) and low-birefringence fibers (LBFs) were analyzed the twist effects [23,24]. Twist effect on the fiber is one of the major causes of the circular birefringence in the fibers. For the case of HBF, the linear birefringence is greater than circular birefringence induced by the twist effect. Thus the twisted fiber acts as a rotator. The circular birefringence caused by the twist effects will be greatly swamped by the large linear birefringence of HBF itself [25]; While the circular birefringence caused by the twist effects and the linear birefringence are co-working in LBF, hence torsion sensitivity of the twist sensor based on LBF can be achieved to be more higher than the one based on HBF. By fixing one end of the fiber and twisting on the other end, the retardance $\Phi_R(\theta)$ between the two guided modes is expressed as a function of twist angle θ which is given as [25]:

$$\Phi_R(\theta) = 2\sin^{-1}\left(\frac{\rho}{\sqrt{1+\rho^2}}\sin\gamma z\right) \quad (2)$$

Here $\rho = \Delta\beta/[2(\theta-\alpha)]$, $\gamma = \sqrt{(\Delta\beta/2)^2 + (\theta-\alpha)^2}$, $\Delta\beta$ is the birefringence of the fiber, z is the twisted fiber length, α is the strain induced optical rotation which is proportional to θ and given as: $\alpha = g\theta$, where g is a constant which depends on the photoelastic coefficients of the material. When the fiber is twisted, the fringe will be shifted due to the extra circular birefringence and phase difference $\Phi_R(\theta)$ caused by the twist. In a certain twist range, $\Phi_R(\theta)$ is direct proportional to the twist angle θ. The twist-induced circular birefringence is proportional to the twist rate applied, and the direction of the circular birefringence vector is determined by the twist direction [25]. Furthermore, the twist induced effective index changes in the fundamental core mode and the cladding supermodes are dependent on the direction of the circular birefringence vector. Thus the right or left-rotatory circular birefringence could result in the effective index difference changing between two modes oppositely, i.e., increasing or decreasing. Consequently, the resonant wavelength shifted linearly toward the longer wavelength as the fiber was twisted anticlockwise and the opposite process occurred as the fiber was twisted clockwise. Therefore, when

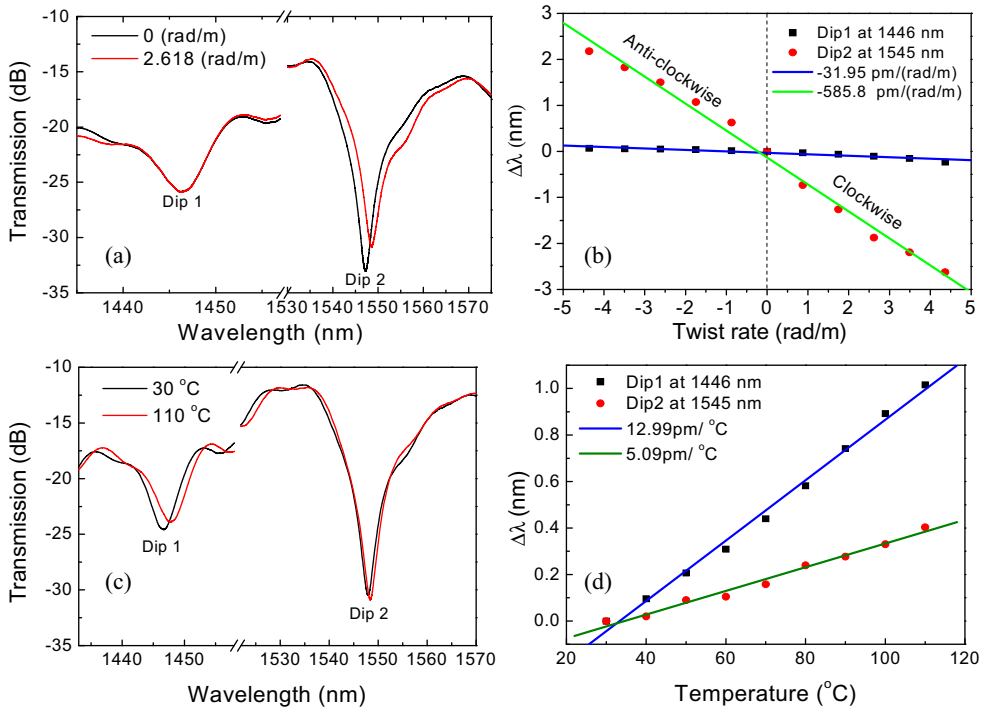

Fig. 6. Shifts of dips against physical parameter and sensitivity of modal interferometer: (a) Transmission spectra of dips at two anti-clockwise twist rates of 0 and 2.618 rad/m.; (b) Dip wavelength shift $\Delta\lambda$ against twist rate applied; (c) Transmission spectra of dips at temperature of 30 and 110 degree; (d) Dip wavelength shift $\Delta\lambda$ against temperature applied.

the fiber was twisted clockwise or anticlockwise, the resonant wavelength shifted toward two opposite directions, and the absolute value of the wavelength shift is proportional to the twist rate applied. The twist direction can be detected by distinguishing whether dips are blueshift or redshift.

In the temperature measurement, we heated the above modal interferometer by using a temperature digital controlled heater, and the temperature ranged from 30 to 110 °C at an interval of 10 °C. Fig. 6(c) shows the transmission spectra of the modal interferometer at the temperature of 30 and 110 °C. It can be seen that the wavelength shift of Dip 2 is more remarkable than that of Dip 1. The relationship of wavelength shift with temperature is shown in Fig. 6(d), Dip 1 and Dip 2 are both linearly redshift as temperature increased. The sensitivities of 12.99 pm/°C for Dip 1 and 5.09 pm/°C for Dip 2 shown in Fig. 6(d) are achieved by linear fitting. It is in the same low level with the results reported in [15] and [21] based on Sagnac interferometer. When considering ambient temperature of EHC-PBGF rises, the two sets of interferences are both affected. While thermo-optic coefficient and the photoelastic coefficient of bar-type silica rods are both higher than those of hollow air core, so the temperature sensitivity of Dip 1 is higher than that of Dip 2.

Considering dips are blueshift due to clockwise twist while dips are redshift along with temperature increased, the achieved sensitivities of this proposed twist sensor are labeled by $S_{T1} = -31.95$ pm/(rad/m) for Dip 1 and $S_{T2} = -585.8$ pm/(rad/m) for Dip 2; temperature sensitivities of Dip 1 and Dip 2 are labeled by $S_{Tem1} = 12.99$ pm/°C and $S_{Tem2} = 5.09$ pm/°C, respectively. The relationship of two dips shift $\Delta\lambda 1$ and $\Delta\lambda 2$ with the variation of twist ΔT and temperature ΔTem can be obtained by a matrix shown in Eq. (3). Then sensing matrix can be determined through a matrix transposition to simultaneously measure the variation of twist ΔT and temperature ΔTem from the shifts of two dips, as following in Eq. (4). And here we can also detect twist direction by distinguishing whether dips are blueshift or redshift.

$$\begin{bmatrix}\Delta\lambda_1\\ \Delta\lambda_2\end{bmatrix} = \begin{bmatrix}S_{T1} & S_{Tem1}\\ S_{T2} & S_{Tem2}\end{bmatrix}\begin{bmatrix}\Delta T\\ \Delta Tem\end{bmatrix} = \begin{bmatrix}-31.99 & 12.99\\ -585.8 & 5.09\end{bmatrix}\begin{bmatrix}\Delta T\\ \Delta Tem\end{bmatrix} \tag{3}$$

$$\begin{bmatrix}\Delta T\\ \Delta Tem\end{bmatrix} = \frac{1}{S_{Tem1}S_{T2}-S_{Tem2}S_{T1}}\begin{bmatrix}-S_{Tem2} & S_{Tem1}\\ S_{T2} & -S_{T1}\end{bmatrix}\begin{bmatrix}\Delta\lambda_1\\ \Delta\lambda_2\end{bmatrix} = \begin{bmatrix}0.68 & -1.74\\ 78.7 & -4.3\end{bmatrix}\begin{bmatrix}\Delta\lambda_1\\ \Delta\lambda_2\end{bmatrix} \tag{4}$$

We also investigated the sensitivity of the above modal interferometer to strain. The dependence of wavelength on strain is shown in Fig. 7. The applied strain ranged from 0 to 3000 με and the strain sensitivity is measured to be −0.267 pm/με for Dip 1, while for Dip 2, it is −0.066 pm/με, this value is 12 times smaller than that measured by using Sagnac interferometer [21], and 9 times smaller than in-fiber polarimeters [20]. We consider it is related to the fact that the low elasto-optical coefficient of air core. For Dip 2 the

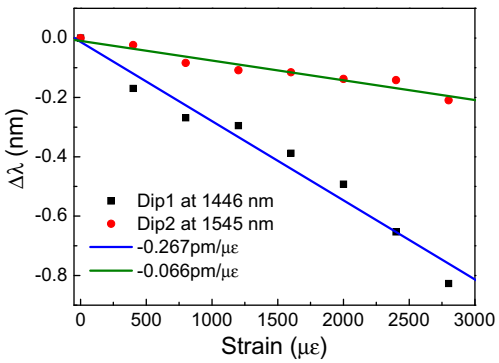

Fig. 7. The relationship of wavelength against strain.

twist measurement error resulting from strain is about 1.13×10^{-4} (rad/m)/με, we think it is small enough to be negligible in the measurement of twist.

4. Conclusion

A novel and simple sensor based on fiber-optic modal interferometer fabricated by a segment of EC-PBGF for simultaneous temperature and twist measurements is demonstrated. Meanwhile the sensor can also measure the twist angle and determine the twist direction simultaneously. Utilizing the obvious difference of two transmission dips on the temperature and twist, two parameters can be distinguished and measured simultaneously by using one single modal interferometer. Meanwhile the low sensitivity to the axial strain makes it the advantage of avoiding the crosstalk of strain in the twist sensing applications.

Conflict of interest

The authors declare no conflict of interest.

Acknowledgements

This work was funded by the National Natural Science Foundation of China (NSFC) under Grants No. 61275125, 61007054, 61308055, National High Technology Research and Development Program of China under Grant No. 2013AA031501 & 2012AA041203. Shenzhen Science and Technology Project (NO. JC201005280473A, JC2011-04210019A, ZDSY 2012061209 4753264, JCYJ 2013-0326113421781, JCYJ 20120613105141482) and Specialized Research Fund for the Doctoral Program of Higher Education (SRFDP, 20124408120004).

References

[1] D.A. Jackson, Monomode optical fibre interferometers for precision measurement, J. Phys. E: Sci. Instrum. 18 (1985) 981–1001.
[2] P. Zu, C.C. Chan, Y.X. Jin, T.X. Gong, Y.F. Zhang, L.H. Chen, X.Y. Dong, A temperature insensitive twist sensor by using low-birefringence photonic-crystal-fiber-based Sagnac interferometer, IEEE Photon. Technol. Lett. 23 (2011) 920–922.
[3] H.Y. Fu, S.K. Khijwania, H.Y. Tam, P.K. Wai, C. Lu, Polarization-maintaining photonic-crystal-fiber-based all-optical polarimetric torsion sensor, Appl. Opt. 49 (2010) 5954–5958.
[4] D. Lesnik, D. Donlagic, In-line, fiber-optic polarimetric twist/torsion sensor, Opt. Lett. 38 (2013) 1494–1496.
[5] D.E. Ceballos-Herrera, I. Torres-Gómez, A. Martínez-Ríos, L. García, J.J. Sánchez-Mondragón, Torsion sensing characteristics of mechanically induced long-period holey fiber gratings, IEEE Sens. J. 10 (2010) 1200–1205.
[6] T. Zhu, K.S. Chiang, Y.J. Rao, C.H. Shi, Y. Song, M. Liu, Characterization of long-period fiber gratings written by CO_2 laser in twisted single-mode fibers, J. Lightwave Technol. 27 (2009) 4863–4869.
[7] Y.P. Wang, J.P. Chen, Y.J. Rao, Torsion characteristics of long-period fiber gratings induced by high-frequency CO_2 laser pulses, J. Opt. Soc. Am. B 22 (2005) 1167–1172.
[8] L.L. Shi, T. Zhu, Y.E. Fan, K.S. Chiang, Y.J. Rao, Torsion sensing with a fiber ring laser incorporating a pair of rotary long-period fiber gratings, Opt. Commun. 284 (2011) 5299–5302.
[9] P. Zu, C.C. Chan, L.W. Siang, Y.X. Jin, Y.F. Zhang, L.H. Fen, L.H. Chen, X.Y. Dong, Magneto-optic fiber Sagnac modulator based on magnetic fluids, Opt. Lett. 36 (2011) 1425–1427.
[10] A.S. Wu, X. Nie, M.C. Hudspeth, W.W. Chen, T.-W. Chou, D.S. Lashmore, M.W. Schauer, E. Towle, J. Rioux, Carbon nanotube fibers as torsion sensors, Appl. Phys. Lett. 100 (2012) 201908-1–201908-4.
[11] R. Gao, Y. Jiang, S. Abdelaziz, All-fiber magnetic field sensors based on magnetic fluid-filled photonic crystal fibers, Opt. Lett. 38 (2013) 1539–1541.
[12] R.F. Cregan, B.J. Mangan, J.C. Knight, T.A. Birks, P. St, J. Russell, P.J. Roberts, D.C. Allan, "Single-mode photonic bandgap guidance of light in air", Science 285 (1999) 1537–1539.
[13] X. Chen, M.J. Li, N. Venkataraman, M.T. Gallagher, W.A. Wood, A.M. Crowley, J.P. Carberry, L.A. Zenteno, K.W. Koch, Highly birefringent hollow-core photonic bandgap fiber, Opt. Express 12 (2004) 3888–3893.
[14] S.S. Mishra, V.K. Singh, Polarization maintaining highly birefringent small mode area photonic crystal fiber at telecommunication window, J. Microw. Optoelectron. Electromagn. Appl. 10 (2011) 33–41.
[15] S.H. Aref, R. Amezcua-correa, J.P. Carvalho, O. Frazão, P. Caldas, J.L. Santos, F.M. Araújo, H. Latifi, F. Farahi, L.A. Ferreira, J.C. Knight, Modal interferometer based on hollow-core phonic crystal fiber for strain and temperature measurement, Opt. Express 17 (2009) 18669–18675.
[16] H.Y. Choi, K.S. Park, S.J. Park, U.C. Paek, B.H. Lee, E.S. Choi, Miniature fiber-optic high temperature sensor based on a hybrid structured Fabry-Pérot interferometer, Opt. Lett. 33 (2008) 2455–2457.
[17] Y.J. Rao, M. Deng, D.W. Duan, T. Zhu, In-line fiber Fabry-Pérot refractive-index tip sensor based on endlessly photonic crystal fiber, Sens. Actuators, A 148 (2008) 33–38.
[18] Q. Shi, F.Y. Lv, Z. Wang, L. Jin, J.J. Hu, Z.Y. Liu, G.Y. Kai, X.Y. Dong, Environmentally stable Fabry-Pérot-type strain sensor based on hollow-core photonic bandgap fiber, IEEE Photon. Technol. Lett. 20 (2008) 237–239.
[19] Y.P. Wang, W. Jin, J. Ju, H.F. Xuan, H.L. Ho, L.M. Xiao, D.N. Wang, Long period grating in air-core photonic bandgap fibers, Opt. Express 16 (2008) 2784–2790.
[20] H. Xuan, W. Jin, M. Zhang, J. Ju, Y. Liao, In-fiber polarimeters based on hollow-core photonic bandgap fibers, Opt. Express 17 (2009) 13246–13254.
[21] G. Kim, T.Y. Cho, K. Hwang, K. Lee, K.S. Lee, Y.G. Han, S.B. Lee, Strain and temperature sensitivities of an elliptical hollow-core photonic bandgap fiber based on Sagnac interferometer, Opt. Express 17 (2009) 2481–2486.
[22] S.H. Liu, N.L. Liu, M.X. Hou, J.T. Guo, Z.H. Li, P.X. Lu, Direction-independent fiber inclinometer based on simplified hollow core photonic crystal fiber, Opt. Lett. 38 (2013) 449–451.
[23] H.M. Kim, T.H. Kim, B. Kim, Y. Chung, Temperature-insensitive torsion sensor with enhanced sensitivity by use of a highly birefringent photonic crystal fiber, IEEE Photon. Technol. Lett. 22 (2010) 1539–1541.
[24] O. Frazao, S.O. Silva, J.M. Baptista, J.L. Santos, G. Statkiewicz-Barabach, W. Urbanczyk, J. Wojcik, Simultaneous measurement of multiparameters using a Sagnac interferometer with polarization maintaining side-hole fiber, Appl. Opt. 47 (2008) 4841–4848.
[25] A. Barlow, J. Ramskov-Hansen, D. Payne, Birefringence and polarizationmode-dispersion in spun single-mode fibers, Appl. Opt. 20 (1981) 2962–2968.